Surface Science 202 (1988) 32–57
North-Holland, Amsterdam

MODELLING THE EFFECT OF CHANGES IN DEFECT GEOMETRY ON CHEMICALLY ACTIVE SURFACES BY THE BOUNDARY ELEMENT TECHNIQUE

Anthony P. PEIRCE

Program in Applied and Computational Mathematics, Princeton University, Princeton, NJ 08544, USA

and

Herschel RABITZ

Department of Chemistry, Princeton University, Princeton, NJ 08544, USA

Received 15 December 1987; accepted for publication 31 March 1988

The boundary element (BE) technique is used to analyze the effect of defect structures upon desorption processes on two-dimensional chemically active surfaces. The standard BE algorithm for diffusion is modified to incorporate the effects of bulk desorption, and an explicit scheme is proposed for the treatment of the non-linear equations associated with localized defect structures. The BE algorithm proposed here provides an elegant representation of the effects of localized non-linear reactions which allows arbitrarily oriented defect structures to be modelled without having to perform mesh deformation.

A class of trapping reactions is assumed to occur along defect structures, and the effect of changes in defect geometry on the balance between the desorptive processes is explored. A number of interesting competitive/cooperative phenomena are observed to occur for the various shapes of defect geometry, including strong intrinsic competition in circular defect structures that form islands of nearly constant concentration, a redistribution of material along V-shaped defect structures in a way that reflects relative competitiveness of defects on opposite sides of the defect structure, and a reduction of competitiveness for defect distributions that are less regular in shape.

The proposed BE algorithm is shown to provide a useful technique for modelling the effect of defect structures on chemically active surfaces.

1. Introduction

Recently the need to understand the influence of defect structures on catalytic phenomena has become important. Practical catalytic reactors are likely to contain active surfaces with high coverages of defect structures due to faulting or foreign substances.

A number of different theoretical analyses of the effect of defect structures in an environment of diffusion, adsorption, and desorption have been considered. Serri et al. [1] have used a discrete step approach to analyze the effect of

0039-6028/88/$03.50

defect structures on desorption kinetics. A more macroscopic analysis of the effect of defect structures assumes that the number of inter-defect sites is sufficiently large for a continuum approximation to be valid. The current authors [2] have demonstrated that the continuum assumption is remarkably good even when the number of inter-defect atomic sites is as low as 20. Analyses based on the continuum assumption include a linear boundary-condition-reaction model that was used to consider the effect of a single defect [3], an effective medium approach that was used to consider the reaction between a single species and a set of randomly distributed reaction sites [4], far from equilibrium phenomena that have been investigated for a single active site in an infinite medium [5], and cooperative instability phenomena that have been investigated for arrays of catalytic sites [6].

Numerical studies of continuum models of defect structures include the use of the multigrid finite difference method with elongated Gaussian representations of defect structures to determine the steady states of a system involving diffusion, adsorption, and many species [7]; as well as the use of an alternating direction implicit (ADI) finite element method for the time dependent analysis of defect structures also represented by elongated Gaussian [8]. In both of these analyses the representation of defects at arbitrary locations in the domain without significant mesh deformations is difficult. A recent approach to this problem [9] has been the use of the boundary element (BE) method to represent defect structures on one-dimensional surfaces on which linear diffusion–desorption processes occur.

In this paper we extend the BE analysis of such problems to two-dimensional surfaces. The BE technique essentially analytically inverts the linear differential operator that describes the bulk diffusion and desorption processes. This results in an integral equation that uses the Green's function for the diffusing–desorbing bulk to provide an elegant representation of the localized non-linear reactions.

The BE algorithm discussed in this paper differs from existing BE formulations [10–12] in two essential features. Firstly, the effect of bulk desorption has to be incorporated into the Green's function. Asymptotic methods are used to evaluate self-effects at defect sites and boundary points. Secondly, the non-linear reactions at defect structures result in an additional term being added to the standard BE formulation for heat conduction. This separation of linear and non-linear terms in the integral equation enables the effects of defect structures to be incorporated in the model without having to disturb the mesh used to propagate the linear part of the solution. This overlay feature is particularly useful if the effects of randomly distributed defects are to be included [7]. In another paper [13], the convergence properties of the BE technique have been examined both with and without localized non-linear reactions.

The proposed BE algorithm will be used in this paper to investigate the

effect of defect structure geometry on the desorption processes taking place on two-dimensional surfaces. We consider reaction terms along the defect structures that model reactive trapping at defects in which the defect structures act as sinks of material that ultimately desorbs as a chemical product. We investigate cooperative/competitive phenomena that take place between the defect structures of a variety of geometrical shapes. A number of interesting phenomena occur in the case of the two-dimensional defect structures that did not occur in the case of one-dimensional defects.

This paper is organized as follows: Section 2 introduces the governing equations of the continuum defect model. In section 3 we discuss the boundary integral formulation of the problem, the space–time discretization, the time-marching of the solution, and the explicit treatment of non-linear effects due to defect structures. In section 4 we use the BE algorithm to investigate the effect of the geometry of defect structures upon desorption processes on chemically active surfaces. Both competitive and cooperative regimes of defect interaction are considered. In section 5 we summarize the results and make some concluding remarks.

2. Governing equations

2.1. The diffusion-localized reaction equation

The equations governing diffusion, adsorption–desorption and localized reaction on the region $\mathscr{S}$ of a catalytic surface are taken to be [5,6]

$$\frac{\partial u}{\partial t} = D\nabla^2 u - \Omega u + f + \sum_{l=1}^{L} R_l(u)\delta(x - x_l(p)), \quad x,\, x_l \in \mathscr{S} \subset \mathbb{R}^2. \tag{2.1}$$

Here $u \in \mathbb{R}^{+s}$ is a vector of positive valued components of the concentrations of the s different species, D is a matrix of diffusion coefficients, Ω is a matrix representing bulk desorption or linear bulk reaction, the vector function $R_l(u)$ is the rate term due to the reactions which occur at the defect structure located on the curve C_l with parametric representation $x_l(p)$, and f is the incident flux of material. In this paper we assume that the bulk is homogeneous so that D and Ω are constant and that the bulk processes are decoupled so that D and Ω are diagonal. As a matter of notational convenience no particular symbol is used to distinguish vectors from matrices. In situations where confusion might result or a listing of the elements of a particular object is required, the appropriate indices are introduced.

In order to be able to determine the solution u of (2.1) we prescribe an initial condition

$$u(x, 0) = u^0(x) \tag{2.2a}$$

and in this paper we typically assume zero flux boundary conditions:

$$\partial u/\partial n \,|_{\Gamma} = 0, \tag{2.2b}$$

where Γ is the boundary of $\mathcal{S}$.

Physically these equations represent the generally non-linear reaction processes that occur at faults or defect structures in the form of arbitrary curves C_l on the surface $\mathcal{S}$ on which adsorption–desorption and linear diffusion take place. This model provides a continuum counterpart of the discrete step model used by Serri et al. [1] to analyze the effect of defects on the desorption of NO from Pt(111) surfaces.

2.2. *Localized reactions representing reactive trapping by defects*

In this paper we consider reaction terms $R_l(u)$ that model reactive trapping at defects in which the defect structures act as sinks of material that ultimately desorbs as a chemical product. There are thus two types of desorptive processes that take place on the surface: the bulk desorption that occurs throughout the surface $\mathcal{S}$ as represented by the term $-\Omega u$ in (2.1), and the desorptive effect due to reactive trapping that takes place at defect structures on the surface. Since material is conserved, the steady state total desorption rate is just f – the rate of adsorption of material to the surface, assuming that the reaction causes no net change on the total moles of all species together. Therefore, the interesting quantity in the above situation is not the total desorption rate but the subdivision of the desorption between the two desorptive processes described above. As a measure of this balance we consider the average bulk desorption rate defined by:

$$\mathcal{D} = \frac{1}{A}\int_{\mathcal{S}} \Omega u(x)\, \mathrm{d}s(x), \tag{2.3}$$

where A is the area of the surface.

In order to avoid confusion in the analysis that follows, the bulk desorption process is referred to as the desorption and the defect desorption process is referred to as reactive trapping.

The reactive trapping models that we consider in this paper are members of the class of reactions of the form:

$$R_i(u_j) = -\prod_{k=1}^{s} (\mathcal{U}_{ki} - u_k)^{\alpha_{ki}} u_i, \quad i,\ j = 1,\ldots,s. \tag{2.4}$$

The features of this model include an increased trapping effect of the ith species with u_i when $u_k \ll \mathcal{U}_{ki}$, a reduced trapping effect in the region $u_k = \mathrm{O}(\mathcal{U}_{ki})$ due to saturation, and complete saturation for the ith species when $u_i = \mathcal{U}_{ki}$. The parameter α_{ki} is used to control the importance of the saturation effect of the kth species on the ith species. This parameter can be

used to switch off the saturation effect by assuming $\alpha_{ki} = 0$. In order to take advantage of the analytic results established [14] for the one-species form of (2.4) assuming defect structures that are essentially one-dimensional, we consider only the one species form of (2.4). More complex members of the class (2.4) also exhibit [9] the same competitive/cooperative behavior as the one-species model.

3. The boundary element (BE) algorithm

In this section we describe the boundary element technique for the solution of the linear diffusion equation with desorption on two-dimensional surfaces on which generally non-linear reactions occur at defect structures. The formulation will be quite general, while the discretization procedure will be outlined for rectangular domains. This analysis is sufficient for the problems considered in this paper.

3.1. The boundary integral formulation of the diffusion-localized reaction equation

The starting point of this formulation is the application of the method of Green's functions to rewrite (2.1) as an integral equation involving boundary values of the solution and its normal derivative, initial values, and sources that are distributed throughout the surface $\mathscr{S}$. As this technique is standard [10–12] the derivation will be omitted. We define

$$\gamma(x) = \begin{cases} 0, & x \notin \mathscr{S}, \\ 1, & x \in \mathscr{S}, \\ \frac{1}{2}, & x \in \Gamma, \end{cases}$$

and rewrite (2.1) and (2.2) in the boundary integral form:

$$\begin{aligned} \gamma(x)u(x,t) = {} & \int_{\mathscr{S}} G(x-\xi, t)u^0(\xi)\, \mathrm{d}s(\xi) \\ & + \int_0^t \int_\Gamma \Big[G(x-\xi, t-\tau) D \frac{\partial u}{\partial n}(\xi, \tau) \\ & - \frac{\partial G}{\partial n}(x-\xi, t-\tau) Du(\xi, \tau) \Big] \mathrm{d}\Gamma(\xi)\, \mathrm{d}\tau \\ & + \int_0^t \int_{\mathscr{S}} G(x-\xi, t-\tau) f(\xi, \tau)\, \mathrm{d}s(\xi)\, \mathrm{d}\tau \\ & + \int_0^t \sum_{l=1}^{L} \int_{C_l} G(x-x_l(p), t-\tau) R_l(u(x_l(p), \tau))\, \mathrm{d}p\, \mathrm{d}\tau. \end{aligned} \tag{3.1}$$

Here

$$\left(D\nabla_\xi^2 - \Omega - I\frac{\partial}{\partial \xi}\right)G(\xi - x, \tau - t) = -\delta(\xi - x)\delta(\tau - t)I,$$

where G satisfies the boundary condition $G \to 0$ as $|x| \to \infty$ and the causality condition $G(x, t) = 0$ if $t < 0$. The explicit expression for G can be derived using Laplace or Fourier transforms [15,16]:

$$G_{ij}(x, t) = H(t)\frac{\exp[-\Omega_i t - r^2/4D_i t]}{4\pi D_i t}\delta_{ij}, \quad i, j = 1, \ldots, s,$$

$$H(t) = \begin{cases} 1, & t \geq 0, \\ 0, & t < 0. \end{cases} \tag{3.2}$$

Here $r = (x_1^2 + x_2^2)^{1/2}$. It should be noted that the Green's function (3.2) differs from that for the standard diffusion equation through the desorption term $\exp(-\Omega_i t)$. In (3.1) we have assumed that the boundary Γ is smooth. In order to obtain an integral equation valid for points x at which Γ has a discontinuous derivative, a limiting procedure has to be used to determine the appropriate value of $\gamma(x)$.

The solution $u(x, t)$ to (2.1) and (2.2) can be determined from (3.1) by the following procedure. We choose x in (3.1) to be on the boundary curve Γ and along the defect curves C_l to obtain integral equations from which the solution u along Γ and C_l can be determined. Having determined the solution along Γ and C_l, (3.1) can be used to determine the solution throughout the surface $\mathscr{S}$ by direct quadrature. Techniques to obtain the approximate solution to (3.1) by this procedure will be discussed in section 3.2.

Comments:

(1) The reformulation of (2.1) and (2.2) as the integral equation (3.1) and the numerical approximation of this integral equation results in a numerical algorithm with quite different properties from the more standard finite difference and finite element techniques. The convergence properties of this numerical technique have been explored by the current authors [13] for problems with and without non-linear reactive defect structures. This convergence analysis demonstrates that the BE algorithms are extremely stable even if large time-steps are used and provides a theoretical framework for resolving meshing issues such as the appropriate size of time-step and spatial meshing. These results will be applied in this paper to choose the appropriate approximation scheme for the examples considered.

(2) We notice that (2.1) differs from the standard boundary integral equation for linear heat conduction by the presence of the last integral in (3.1), which represents the effect of defect structures on the solution. This separation of linear and non-linear effects enables the effects of defect structures along

arbitrary curves C_l in $\mathcal{S}$ to be incorporated by merely evaluating the last integral in (3.1). This implies that arbitrarily oriented defect structures can be modelled without disturbing the spatial meshing used to evolve the linear part of the solution. Since we are particularly concerned in this paper with the effect of changes in defect geometry on desorptive processes, the overlay feature described above makes the BE technique eminently suited to this task. Since the detailed shapes of the surfaces $\mathcal{S}$ are not of primary importance in this paper, we assume that the surfaces are all rectangular. The only physical criterion is that the boundary Γ of $\mathcal{S}$ be sufficiently far from the defects so as to have a minimal effect on the chemical processes.

3.2. Approximate solution of the boundary integral equations

The approximation scheme commonly used in the BE literature [10–12] to solve the boundary integral equation (3.1) is based on piecewise polynomial collocation. We shall briefly describe this technique and provide the expressions for the required influence matrices in an appendix. The numerical treatment of the non-linear effects of defect structures are not available in the literature and will be discussed in more detail in this section. Some comments will be made about techniques that can be used to make the time evolution of the linear effects on rectangular domains more efficient.

3.2.1. Space–time discretization

The surface $\mathcal{S} = [0, X] \times [0, Y]$ is divided into MN rectangular cells $\mathcal{S}_{mn} = \{(x, y): 2(m-1)a \le x \le 2ma;\ 2(n-1)b \le y \le 2nb\}$ where $2a = X/M$ and $2b = Y/N$. Corresponding to this mesh of space cells the boundary Γ of $\mathcal{S}$ is divided into $2(M+N)$ line segments Γ_q of length $2a$ in the X direction and $2b$ in the Y direction. By a similar procedure to that used for the boundary, defect curves C_l are divided into P_l line segments. Finally, the space time interval $[0, T]$ is divided into J intervals $[t_j, t_{j+1}]$, $j = 0, \ldots, J$.

Over this mesh of space–time cells and elements we construct piecewise polynomials in terms of which the solution u, the initial condition u^0, and the adsorption function are expanded. These expansions are substituted into (3.1) and the products of the Green's function and the piecewise polynomial basis functions are integrated to form the appropriate influence matrices. These influence matrices are then used to evolve the solution from one time-step to the next by a procedure outlined in the next section.

In this paper we have found it sufficient to assume that the solution is piecewise constant over each of the cells, elements, and time-steps. The required influence coefficients are given in appendix A. According to the convergence analysis [13] low degree spatial interpolation is appropriate if we are interested in taking reasonably large time-steps to achieve a steady state solution, which is the case in this paper. For the piecewise constant meshing

strategy adopted in this paper the meshing parameter $\Theta = 2(D\,\Delta t/ab)^{1/2}$ (which was identified in the convergence analysis) should satisfy the minimal consistency requirement $\Theta > 2$. All the meshes used in this paper satisfy this requirement to avoid the phenomenon of numerical diffusion.

3.2.2. Time marching when no defect structures are present

We exploit the Volterra form of the time integrals in (3.1) to construct the following time marching scheme. The solution is carried from one time-step t_j to the next $t_{j+1} = t_j + \Delta t_j$ by using (3.1) in which $t = \Delta t_j$ and the solution values at time t_j are regarded as initial values i.e. $u^0(x) = u(x, t_j)$. In the absence of defect structures we can use the integral equation (3.1) with $x \in \Gamma$ to determine the value of the solution $u(x_q, t_{j+1})$ at the midpoints x_q of the boundary elements Γ_q, $q = 1, \ldots, 2(M+N)$. For problems with no defect structures all the terms on the right-hand side of the discretized form of (3.1) are now known and the solution $u(x, t_{j+1})$ for all $x \in \mathcal{S}$ can be determined from (3.1) by direct quadrature. These values can now be used as initial data for the next step.

In this paper we assume that all the time-steps for a given problem are the same size Δt so that the influence matrices can be precalculated and stored a priori. For the rectangular domains considered in this paper it is necessary to store only abbreviated tables of influence coefficients, which involve of the order of MN real variables per species. Thus in moving from one time-step to the next, the solution is advanced by a procedure that involves mainly matrix multiplication (that is treated explicitly). Only the terms involving the boundary unknowns and active sites have to be solved at every time-step. In the next section we outline a procedure to treat defect structure effects explicitly.

3.2.3. Explicit treatment of the non-linear effects due to defect structures

In this section we propose an iterative predictor corrector sequence to determine the solution of the non-linear equations at the defect structures themselves. Initially we assume that the solution at each defect element is constant over the time-step $[0, \Delta t]$ and equal to its initial value. Having made this assumption only the boundary values of u need to be determined in order to determine an approximate solution throughout $\mathcal{S}$ at time $t = \Delta t$. The new values of u at the defect elements can be used on the right-hand side of (3.1) to determine a new approximate solution $u(x, t)$. This iteration sequence is best used together with some time polynomial interpolation scheme to obtain more and more accurate approximations of the defect structure integrals in (3.1). One such scheme is the piecewise linear Caratheodory iteration sequence [13], which was shown to provide a convergent time evolution scheme for a class of model problems derived from (3.1).

In this paper we use a scheme that assumes the solution u at each defect site is constant over the time-step $[0, \Delta t]$. This amounts to taking only the first step in the above iterative algorithm. This procedure is extremely attractive from a computational point of view as the solution is then taken from one time-step to the next in an explicit fashion and does not require the solution of any non-linear equations. This scheme has been demonstrated [9] to be effective. Errors as small as 2.3% in the transient regime decrease further as time progresses. Since in this paper we are interested in achieving steady state solutions, this choice of scheme to treat non-linear effects at defect structures is appropriate.

4. The effect of defect geometry on desorptive processes

In this section we use the BE algorithm described in section 3 to investigate the effect of the geometry of defect structures on the desorptive processes on chemically active surfaces. We assume that the reactive trapping process described in section 2.2 takes place at the defect structures. The effect of the defect-structure-geometry upon the desorptive processes is assessed by determining the bulk desorption rate $\mathscr{D}$ defined in (2.3). An increase in $\mathscr{D}$ as a result of a change in geometry indicates a lowering of the trapping efficiency of the defect structure, whereas a decrease in $\mathscr{D}$ represents an increase in trapping efficiency.

In order to be able to compare different defect geometries we shall always assume that the same length of defect structure is present on the surface for all the geometries compared, and that all the other parameters are the same in each case. In all the examples considered in this section we consider the one-species form of trapping model (2.4) in which $s = 1$, $\mathscr{U}_{11} = 1$, and $\alpha_{11} = 1$. Finally, the unit surface $\mathscr{S} = [0, 1] \times [0, 1]$ will be used in all the examples considered in this section.

4.1. Competitive behavior between defect structures

In all the examples considered in this subsection we use the following parameter set: $D = 1.0$, $\Omega = 2.0$, $f(x, y) = 0.5$, and $u^0(x, y) = 0.0$. The numerical approximation to (2.1) and (2.2) was obtained using the BE technique described in section 3. A mesh of $M = 25$ by $N = 25$ piecewise constant interior cells was used so that $a = b = 0.02$, and the corresponding $2(M + N) = 100$ boundary elements were used to discretize the boundary. The size of time-step used was $\Delta t = 0.0125$ and the numerical solution was determined out to $t = 2.5$. The minimal consistency requirement $\Theta > 2$ discussed in section 3.2.1 is more than adequately satisfied by the mesh defined above for which the mesh parameter $\Theta = 11.2$.

In this subsection we start with an example of a single line of defects, which forms a reference problem for the remaining examples. This line defect is then considered to be deformed into other defect structures having the same length, and the effect on the desorption rate $\mathscr{D}$ is determined.

4.1.1. A single line of defects

We consider the defect structure in this example to be the line $x = 0.5$; $0 \le y \le 1.0$ as shown in fig. 1. This example is particularly useful as it forms an approximation to a one-dimensional problem for which there is an analytic solution. In particular, if the surface $\mathscr{S} = [0, 1] \times (-\infty, \infty)$ and the above line were extended to infinity, then the steady state solution to (2.1) and (2.2) is independent of y and has the following x dependence:

$$u(x) = \left(u^{\pm}(0) - \frac{f}{\Omega}\right) \frac{\cosh \omega(L - |x|)}{\cosh \omega L} + \frac{f}{\Omega}, \tag{4.1}$$

where $u^{\pm}(0) = \frac{1}{2}(T + 1) \pm \frac{1}{2}[(T + 1)^2 - 4fT/\Omega]^{1/2}$, $\omega = (\Omega/D)^{1/2}$, $T =$

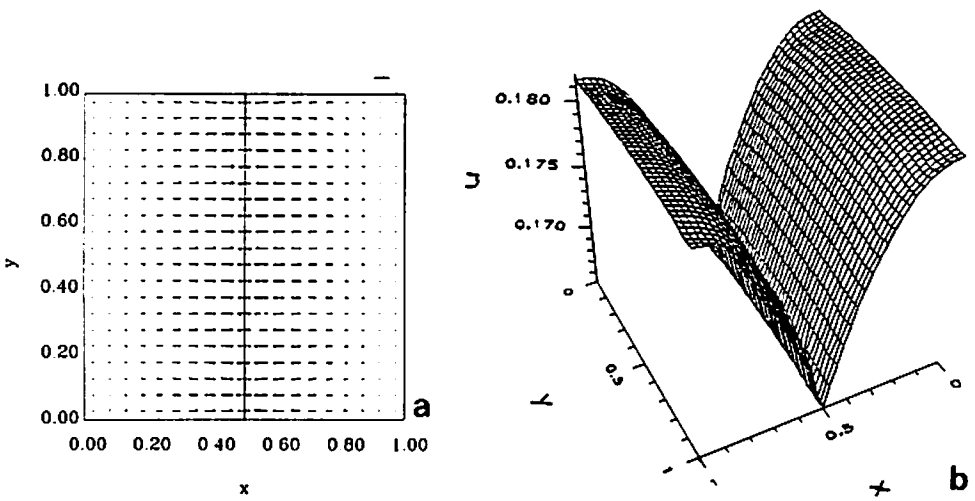

Fig. 1. (a) The flux vectors $-\nabla u$ at $t = 2.5$ are plotted at uniformly distributed points on the unit surface containing a single line defect $x = 0.5$, $0 \le y \le 1$. The flux vectors have been scaled to the largest flux vector, which has the length indicated at the upper right corner of the plot and whose magnitude in this case is 0.067. The flow of material into the line-defect at which reactive trapping occurs can be seen clearly in this diagram. Zero normal flux boundary conditions are considered in this problem. These imply a reflected periodic lattice of line-defects at $x = -0.5, \pm 1.5, \ldots$. The small flux vectors near $x = 0$ and $x = 1$ provide evidence of competition for material between neighboring defects in this lattice. This problem also forms an approximation to the essentially one-dimensional problem in which the defects in the lattice are infinitely long. The analytic solution to the one-dimensional problem is given in eq. (4.1). This case is important as it provides both a reference problem for the other examples in the paper and access to the one-dimensional theory of competitive behavior. (b) The spatial distribution of the concentration over the unit surface at $t = 2.5$. The flow of material into the line-defect can be clearly seen in this plot.

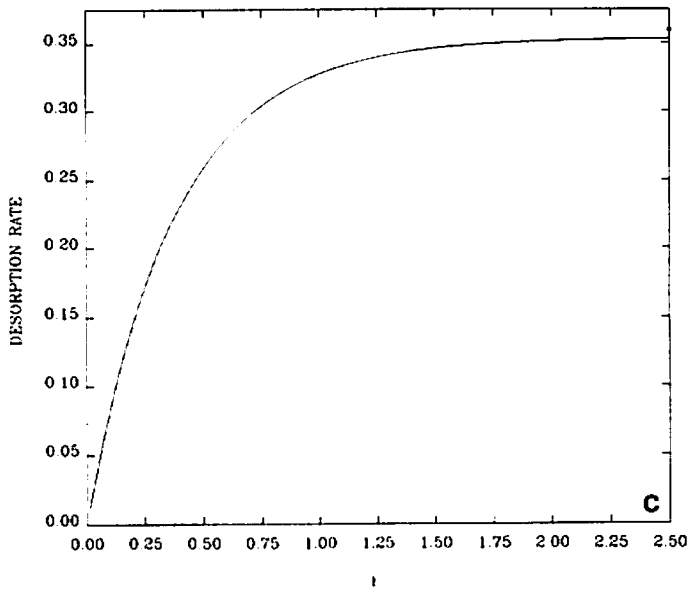

Fig. 1c. The time evolution of the desorption rate $\mathscr{D}$ for the line-defect case shown in 1a. The desorption rate provides a measure of the balance between the bulk desorption process and the desorptive effect due to the reactive trapping at the line defect. The steady state analytic desorption rate is $\mathscr{D} = 0.3598$ and is denoted on the figure by the triangular symbol. The numerical solution yields a desorption rate $\mathscr{D}$ at $t = 2.5$ that is within 2% of the analytic value. In the examples that follow we compare the numerical solution at $t = 2.5$ for various defect structures as if they were at the steady state.

$2\omega D \tanh(\omega L)$, $L = 0.5$, and in this case the line defect is located at $x = 0$. It has been established [14] that provided the solution (4.1) is real then the negative branch $u^{-}(0)$ is always stable.

Using the parameter set for this section the analytic solution given by (4.1) was compared with the approximate BE solution. The approximate BE solution at $t = 2.5$, sampled at the midpoint of the defect line-segment, was within 2% of the exact steady state (i.e. $t \to \infty$) solution given by (4.1).

Not only does this example provide a useful test of the numerical algorithm, but it also serves as a reference problem in terms of which the theory for cooperative behavior established for one-dimensional problems [14] can be applied. In particular, since $R'(u(0)) = -1 + 2u(0) < 0$ in this case, the one-dimensional theory predicts competitive behavior [14] between perturbed defects. These one-dimensional perturbations comprise parallel translations of the infinitely long line defects for which the one-dimensional theory applies. In this paper we are able to consider a larger variety of defect perturbations owing to the additional freedom introduced by the two-dimensional surfaces considered.

Also plotted in fig. 1a is the flux vector $-\nabla u$ at uniformly distributed points (x_m, y_n) on $\mathscr{S}$. The flow of material into the line defect can be clearly seen in this representation. All the flux vectors have been scaled to the largest flux vector that has the length indicated at the right corner of the plot and whose magnitude in this case is

$$\max_{(x_m, y_n)\in\mathscr{S}} |\nabla u| = 0.067.$$

In fig. 1b the spatial concentration distribution over the surface $\mathscr{S}$ is plotted. The trapping effect of the line defect causes a drop in the concentration in the vicinity of the defect. The artificial corners in the numerical model introduced by replacing the infinitely long line defect (assumed in the case of the analytic solution (4.1)) by a finite line segment with zero flux boundary conditions on a square domain introduce small errors. These errors can be observed by the non-parallel flux vectors in (a) in the immediate vicinity of the boundary segments $y = 0.0$ and $y = 1.0$, and by the drop in concentration in (b) in the vicinity of the corners.

Since there is a zero normal flux boundary condition along Γ and in particular along the lines $x = 0.0$ and $x = 1.0$, we observe that there is an implied periodic lattice of defect lines at $x = -0.5, \pm 1.5, \ldots$. Competition for material to trap occurs between the line defects in this implied lattice, which manifests itself in the small flux vectors in (a) and the local maxima of u at $x = 0.0$ and $x = 1.0$. In order that competition for material by defect structures reflected across the zero flux boundaries remain sub-dominant to the local competitive effects, we shall limit the defect structures that are deformations of the line segment of this section to regions remote from the boundary Γ.

In fig. 1c the time evolution of the average desorption rate $\mathscr{D}$ defined in (2.3) is plotted. Since the desorption rate from the surface is proportional to the concentration u, we observe that the material on the surface increases rapidly until the steady state concentration is approached. From fig. 1c it can be seen that the solution is close to the steady state after $t = 2.50$. In fact, the value of the steady state ($t \to \infty$) average desorption rate is $\mathscr{D} = 0.3598$ while the value obtained from the numerical solution is $\mathscr{D}(t = 2.5) = 0.3530$, which constitutes a difference of 1.9%. Since the numerical solution has not been determined for a particularly large value of t we expect that the actual numerical error is much less than this. However, for our purposes the value of the desorption rate at $t = 2.5$ suffices as the effect of geometric perturbations on the desorption rate will have manifested itself by this time. Therefore, in all the examples that follow we compare the numerical solutions at $t = 2.5$ as if they were at the steady state.

4.1.2. Deformation into a regular and a random distribution of line defects

In this subsection we consider the deformation of the line segment considered in section 4.1.1 into smaller line defect structures in the region $0.2 \leq x, y$

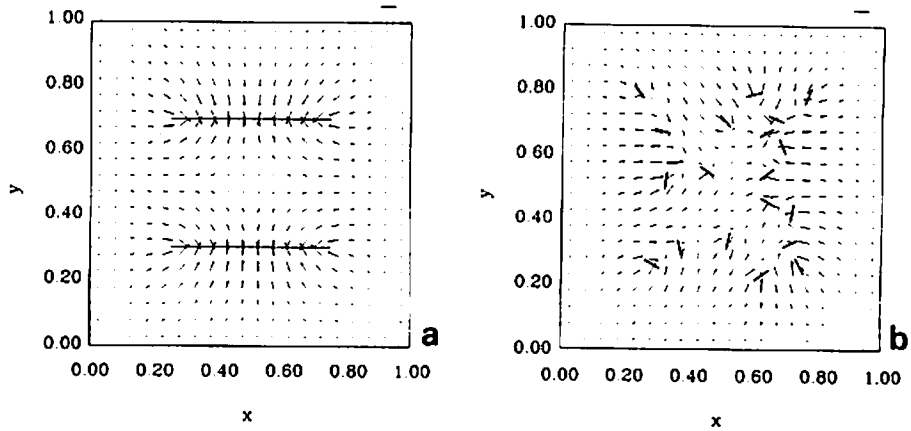

Fig. 2. (a) The flux vectors for the deformation of the reference line-defect into smaller line-defect structures perpendicular to the original defect. As before, the flux vectors are scaled to the maximum flux vector that has a magnitude of 0.060. Evidence of local competitive behavior between the line-defects can be seen by the local maximum that occurs at $(x, y) = (0.5, 0.5)$ and by the small flux vectors in this region. (b) The flux vectors when the line-defect has been redistributed randomly throughout the region $0.2 \leq x, y \leq 0.8$. The maximum flux vector in this case has a magnitude of 0.065. The flow of material is more complex than before. However, it can be seen that material can flow freely into each of the small defect structures without any substantial regions of competition occurring. This defect distribution can therefore be expected to be a relatively efficient trap of material.

≤ 0.8. In fig. 2a the flux vectors are provided for the defect structures comprising two parallel line segments $0.25 \leq x \leq 0.75$, $y = 0.3$ and 0.7. Evidence of local competitive behavior between the line defects in this case can be seen by the local maximum of the concentration that occurs at $(x, y) = (0.5, 0.5)$ and the small flux vectors in this region.

In fig. 2b the flux vectors are provided for the redistribution of the single line defect of section 4.1.1 into 20 smaller defects that are randomly distributed throughout the region $0.2 \leq x, y \leq 0.8$. The flow of material in this situation is far more complex. However, from fig. 2b it can be seen that for this random distribution of defects, flow of material into each of the small defect structures can take place without any substantial regions of competition for material occurring. We would, therefore, expect this defect distribution to be a relatively efficient trap of material.

In fig. 3 the average desorption rate $\mathscr{D}$ for the above two defect structures can be compared with the desorption rate of the line defect as well as the desorption rate of the defect structures from figs. 4 and 5. This enables the effect of local competitive behavior on the trapping efficiency of the various defect structures to be determined. In the case of the parallel defects, the average desorption rate $\mathscr{D}$ can be seen to increase relative to the case of the single line defect owing to the competitive behavior that was observed in fig.

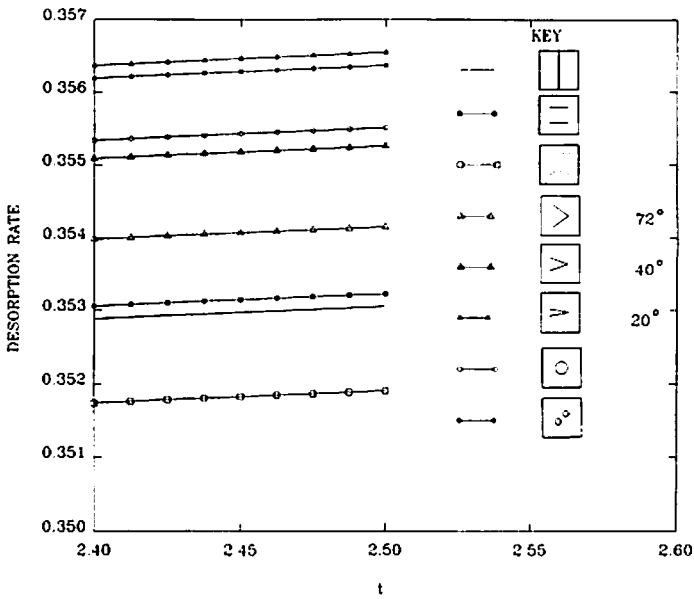

Fig. 3. The average desorption rate $\mathscr{D}$ for all the defect structures considered in figs. 1, 2, 4 and 5 are plotted for comparison. $\mathscr{D}$ provides a measure of the local competitive behavior of the defect structure under consideration. An increase in competitive behavior between the defects in a defect structure reduces the trapping efficiency of the defect structure as a whole, which results in an increase in the average bulk desorption rate $\mathscr{D}$. Of particular interest in this figure is the reduced competitiveness in the case of the randomly distributed defects shown in 2b. This demonstrates the reduced competitive effect that results from a movement away from the more orderly defect structures toward a distribution that is closer to a global minimum.

2a. In contrast $\mathscr{D}$ can be seen to decrease in the case of randomly distributed defects, which is consistent with the free access that material has to the defects, which was observed in fig. 2b. It is interesting to contrast this reduced competition caused by a symmetry breaking perturbation of the defects with the one-dimensional case [14], which comprises parallel translations of infinitely long line defects. In that case symmetry breaking perturbations for this density of defects at this adsorption level were shown to consistently increase competitiveness between defects. In two dimensions we see that there is more freedom in the possible symmetric situations and the types of perturbations. The random defect distribution considered in fig. 2b is thus a movement away from the symmetric parallel lattice distributions towards a distribution that is closer to the global minimum of the desorption rate $\mathscr{D}$.

4.1.3. Deformation into V-shaped defect structures

In this subsection we consider the deformation of the line defect analyzed in section 4.1.1 into V-shaped defect structures having the same length and

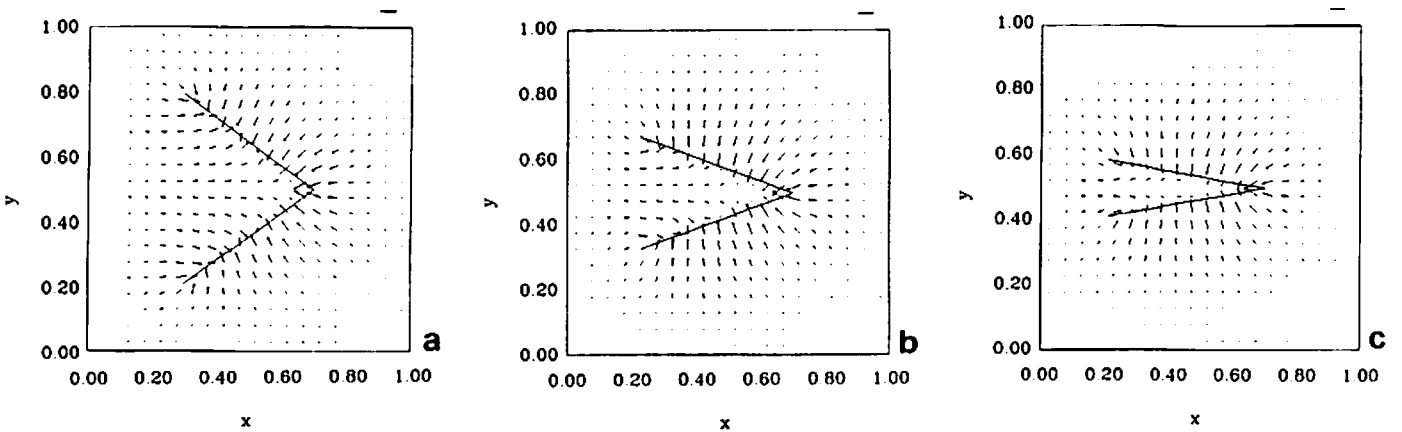

Fig. 4. (a) The flux vectors when the reference line-defect has been deformed into a V-shaped defect structure with the same length and including an angle of 72°. The maximum flux vector in this case has a magnitude of 0.102. Evidence of competition between the sides of the defect structure can be seen from the small vertical component of the flux vectors in this region. (b) The flux vectors for deformation to a V-shaped defect structure with included angle of 40°. The maximum flux vector in this case has a magnitude of 0.114. The same evidence of competition as in (a) can be observed. An interesting phenomenon that can be observed here is the flux of material along the axis of the V away from the vertex. This redistribution of material along the length of the V reflects the relative competitiveness of the defects on opposite sides of the defect structure. (c) The flux vectors for deformation to a V-shaped defect structure with included angle of 20°. The maximum flux vector in this case has a magnitude of 0.151. The same evidence of competition between defects seen in (a) and (b) is observed here. In this case the redistribution of material due to the relative competitiveness of the defects is even more pronounced than in (b).

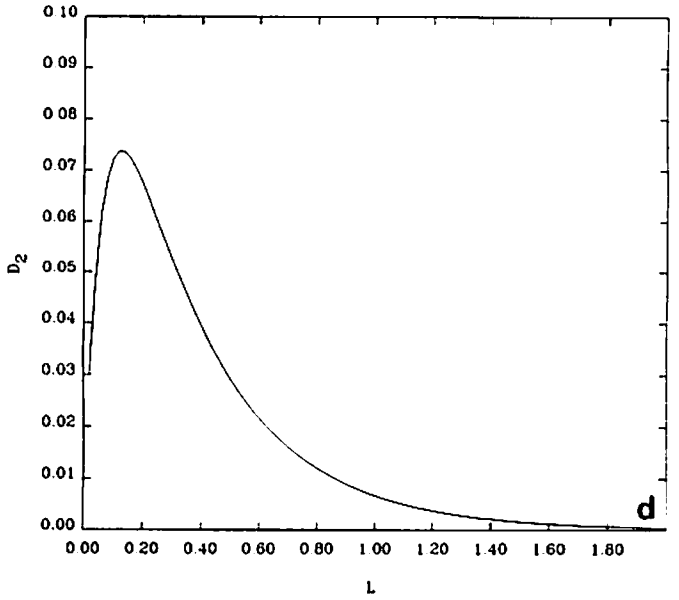

Fig. 4d. The competitiveness (as measured by $\mathscr{D}_2$) of a lattice of one-dimensional defects is plotted as a function of L where $2L$ is the defect spacing. The maximum of this competitiveness curve provides an explanation for the flow in (4b) and (4c) of material along the length of the V-shaped defect structures into a point that is away from the vertices.

subtending angles of 72°, 40° and 20° respectively. The flux vectors for these three cases are plotted in figs. 4a, 4b, and 4c respectively. In each case there is evidence of strong competitive behavior in the region between the two inclined lines. This can be seen by the small positive and negative vertical components of the flux vectors in this region, and the corresponding ridge of the concentration field u that occurs along the line $y = 0.5$.

Another interesting phenomenon that can be seen in fig. 4b is the flux of material within the V away from the vertex at $(x, y) = (0.7, 0.5)$ toward the point $(x, y) = (0.6, 0.5)$. This phenomenon is even more pronounced in fig. 4c in which the material moves toward the point $(x, y) = (0.5, 0.5)$. We make use of the results of the one-dimensional theory [14] in order to provide an explanation for this phenomenon. Firstly, we note that when defects act in close proximity to one another they will naturally compete with one another to a greater or lesser extent. The allocation of material to the defects in such an environment will depend on the relative local competitiveness of the defect structure. An interesting property of the V-shaped defect structures considered in this section is that they are essentially made up of elemental pairs of defects that span a wide range of separations – from zero separation near the vertex to a maximum separation near the edges.

In order to see how competitiveness can vary as the separation between defects changes in an environment of many defects, we consider a one-dimensional periodic lattice of defects having a separation $2L$. To determine how the competitiveness between the defects varies as a function of L, we perturb for a range of values of L one defect in the lattice by an amount ϵ and examine the first non-zero perturbation $\epsilon^2 \mathscr{D}_2$ to the desorption rate $\mathscr{D}$. An increase of $\mathscr{D}_2$ with a change in L indicates an increased competitiveness due to the change in lattice spacing. In fig. 4d the quantity $\mathscr{D}_2$ is plotted as a function of L for the same values of Ω, D, and f considered here. As L is decreased from 1.0 the competitiveness of the defects is increased until a maximum competitiveness is reached at $L \simeq 0.13$. As L is decreased further there is a rapid decrease in competitiveness of the defects in the lattice.

Although the detailed geometry for the V-shaped defect structures is different and therefore precludes quantitative predictions, the phenomenon of a maximum competitiveness for non-zero values of L can be used to provide an explanation for the flux of material away from the vertices of the V-shaped defect structures. Since the V-shaped defect structures span a range of values of L along their length, fig. 4d indicates that defect competition will be extremely small near the vertex, will increase as the observation point is moved away from the vertex along $y = 0.5$, and will eventually decrease as the observation point is moved still further from the vertex. This variation in competitive behavior along the axis of the V-shaped defect structures provides an explanation for the flux of material away from the vertex observed in figs. 4b and 4c.

In fig. 3 the average desorption rate $\mathscr{D}$ for all the V-shaped defect structures can be seen to be higher than that of the reference line defect. This increase is due to enhanced competitive behavior between the V-shaped defect structures. The competitiveness of the V-shaped defect structures is seen to increase as the included angle decreases. The desorption rate $\mathscr{D}$ provides a global measure of the competitiveness of the defect structure as a whole and gives no indication of the relative competitiveness of defects within the defect structures themselves.

4.1.4. Deformation into circular islands

In this subsection we consider the deformation of the line segment analyzed in section 4.1.1 into circular defect structures on $\mathscr{S}$ having the same defect length. In fig. 5a the flux vector representation of the BE solution at $t = 2.5$ is provided for a single circle with a perimeter of 1 centered at $(x, y) = (0.5, 0.5)$. The intrinsic competitive behavior between the defects on the circle has the effect of reducing the flux of material within the circle itself, as can be seen by the small flux vectors in the interior of the circle. We observe that the solution within the circle is virtually uniform, having a maximum value of $u = 0.1662$ at the center of the circle and a typical value of $u = 0.1651$ along the periphery

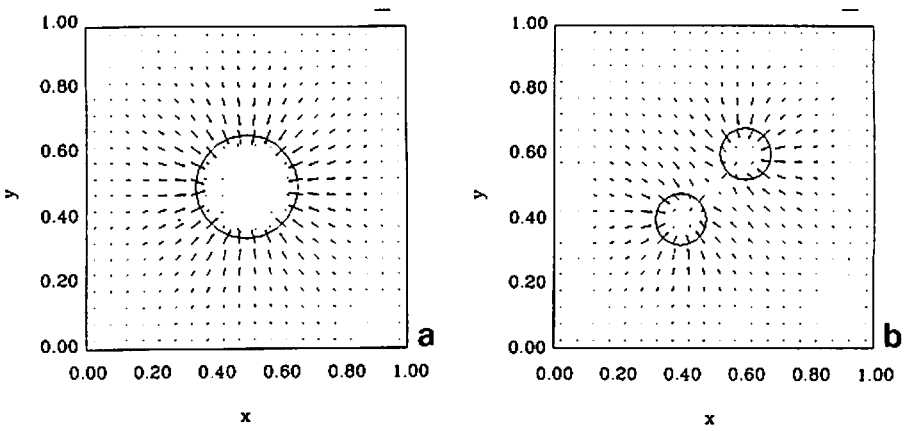

Fig. 5. (a) The flux vectors for the deformation of the reference line-defect into a circular defect structure having the same length. The maximum flux vector in this case has a magnitude 0.108. The small flux vectors in the interior of the circle is evidence of intrinsic competition between the defects on the circle. The defects are also seen to have a shielding effect that results in a near uniform concentration distribution within the circle. Thus the defect structure forms an island of near constant concentration. (b) The flux vectors are plotted for the deformation of the reference line-defect into two neighboring circular defect structures having the same total length. The maximum flux vector in this case has a magnitude 0.096. As was the case in (a) there is evidence of intrinsic competition that manifests itself in the small flux vectors within the circles themselves. Between the defect islands the small flux vectors provide evidence of mutual competition between the defect islands. The small flux of material within each of the circles in the direction of the other circle also provides evidence of mutual competition.

of the circle. Typical values of the solution in the region outside and remote from the circle are $u = 0.181$. Thus the circle of defects has a shielding effect to form an island of nearly constant concentration over which the solution has a negative curvature.

In fig. 5b the flux vectors are plotted for the case of deformation of the line segment into two neighboring circular defect structures. Three regions in which there is evidence of competitive behavior can be observed in this case. As was the case with the single island, the small flux vectors within the circles provides evidence of intrinsic competition among the defects on the periphery of each circle. The third region of competitive behavior occurs between the defect islands in the vicinity of $(x, y) = (0.5, 0.5)$ at which there is evidence of a local maximum of u. More evidence of competitive behavior between the two defect islands can be observed in the small flux of material that occurs within each of the circles in the direction of the other circle.

In fig. 3 the average desorption rate $\mathscr{D}$ for the circular defect structures can be seen to be higher than that of the line defect. This increase is due to enhanced competitive behavior between the circular defect structures, which

reduces the trapping efficiency of the defect structure relative to the case of a single line of defects. The single large circular defect structure is seen to be less competitive than the case of the two neighboring circular defects. The greater competitiveness of the two neighboring circular defect structures is evidence of enhanced intrinsic competition of the two smaller circles and additional extrinsic competition between the two circular defect structures.

4.2. Cooperative behavior between defect structures

In this subsection we consider defect structures that act in a cooperative fashion. In all the examples considered in this subsection we use the following parameter set: $D = 1.0$, $\Omega = 2.0$, $f(x, y) = 1.9$ and $u^0(x, y) \equiv 0.0$. These conditions only differ from those in section 4.1 by an increase in the level of adsorption f which alleviates defect competition for the substance u. Instead of competing, neighboring defects serve to reduce the saturation effect locally, which serves to improve the trapping efficiency of the defect structure as a whole. This mode of behavior we refer to as cooperative.

The discretization strategy used in this subsection is the same as that used in section 4.1. As a reference problem in this subsection we consider two line-defects $x = 0.25$ and 0.75; $0 \le y \le 1$. These line-defects are then deformed into defect structures of various geometries that have the same length. In order to measure the cooperative/competitive effect of these deformations the desorption rate $\mathscr{D}$ defined in (2.3) is determined in each case.

The reference problem in this case also approximates the analytic solution (4.1) obtained by considering infinite line defects. In this case $L = 0.25$ and the one-dimensional theory [14] predicts cooperative behavior between defects that are moved into close proximity to one another.

In fig. 6a the flux vectors are provided for the reference problem comprising two line-defects. In this case, small flux vectors, similar to those found in the previous section, are observed between the line defects. However, they represent an effect that is quite different for the defect structures in this regime. In this regime, defects that are in close proximity to one another reduce the concentration level locally and therefore their mutual level of saturation. This improves the trapping efficiency of the defect structure, which will cause the bulk desorption rate $\mathscr{D}$ to decrease. This local interaction we refer to as cooperative behavior.

In fig. 6b the flux vectors are provided for the deformation of the two line-defects into two neighboring circles. Interior to the circles, regions of small flux vectors similar to those in fig. 5b can be observed due to the shielding effect of the circular defects. Similarly, between the defect islands in the vicinity of the point $(x, y) = (0.5, 0.5)$ there is evidence of a local maximum of u. Since the level of adsorption to the surface is higher in this case than in 5b, competition between the defect structures is alleviated and the

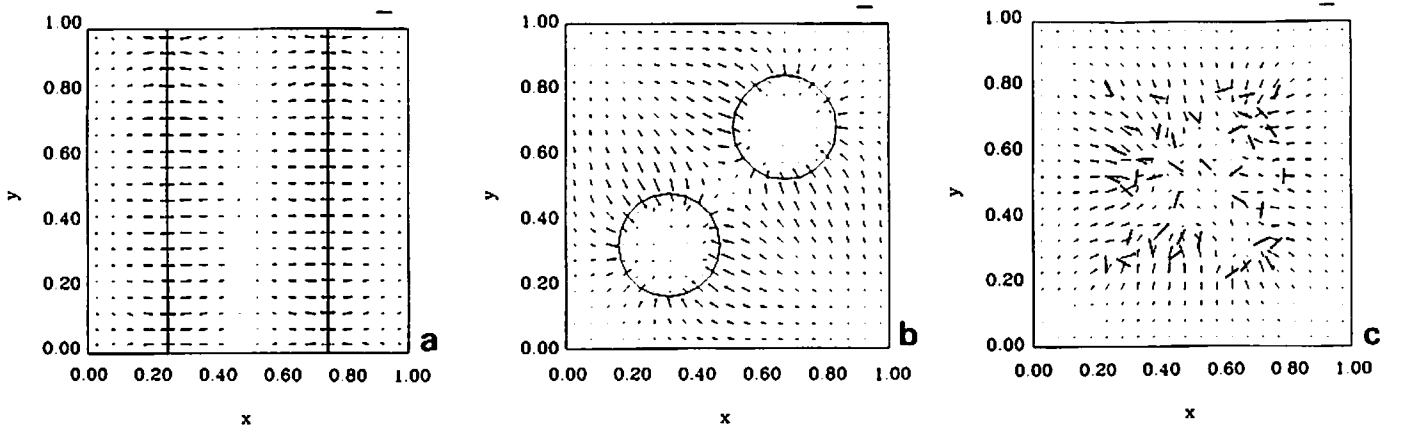

Fig. 6. The parameter set has been chosen in this figure so that the defect structures act in a cooperative fashion. The reference problem in this case comprises two parallel line-defects. The small flux vectors between neighboring defects in this case is evidence of the mutual reduction of concentration locally, which reduces the level of saturation. This improves the trapping efficiency of the defect structure, which will cause the bulk desorption rate $\mathscr{D}$ to decrease. This local interaction we refer to as cooperative behavior. (a) The flux vectors for the reference two line-defect problem. In this case the maximum flux vector has a magnitude of 0.107. The small flux vectors along $x = 0.5$ provide evidence of mutual cooperation. (b) The flux vectors when the reference line-defects are deformed into a single circle of the same length. In this case the maximum flux vector has a magnitude of 0.140. The small flux vectors provide evidence of intrinsic cooperativity of the circular defect structure. (c) The flux vectors when the reference line-defects are broken into 40 smaller defect segments that are randomly distributed throughout the region $0.2 \leq x, y \leq 0.8$. In this case the maximum flux vector has a magnitude of 0.167. The small x components of the flux vectors between the defects in the region $0.2 \leq x \leq 0.4$; $0.2 \leq y \leq 0.8$ and those in the region $0.6 \leq x \leq 0.8$; $0.2 \leq y \leq 0.8$ indicate possible cooperative behavior.

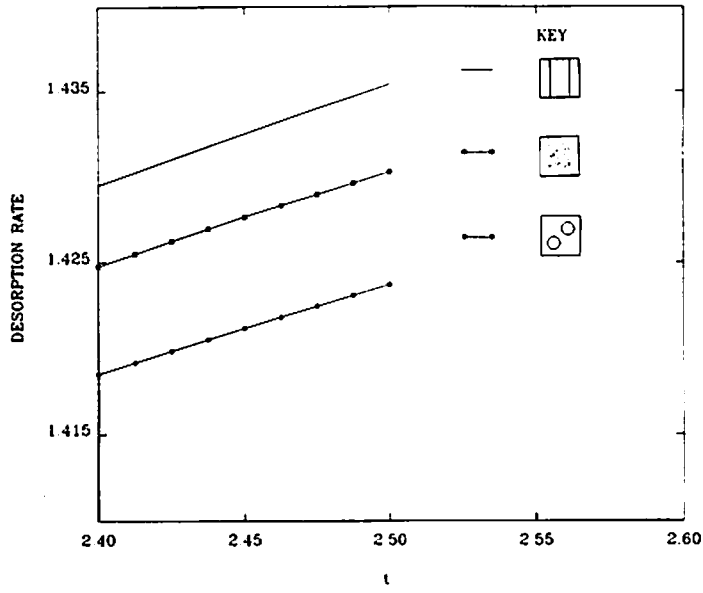

Fig. 7. The average desorption rates $\mathscr{D}$ for all the defect structures considered in fig. 6 are plotted for comparison. In both the case of the circular defect structure and the randomly distributed defects, $\mathscr{D}$ is lower than that of the reference problem comprising two line-defects. In these cases there is an increase in cooperative behavior which enhances the trapping efficiency of the defect structure as a whole and results in a decrease in the bulk desorption rate $\mathscr{D}$.

circular defects are seen to cooperate mutually to reduce the saturation effect. The reduced saturation increases the trapping efficiency of this distribution of defects relative to the two reference line-defects. In fig. 6c the flux vectors are plotted for the situation in which the two parallel defects have broken up into 40 smaller defect segments that are distributed randomly throughout the region $0.2 \leq x,\ y \leq 0.8$. In this situation it is difficult to identify and definite flux patterns. However in the region $5.0 \leq x \leq 6.5$ and $2.5 \leq y \leq 7.0$ the flux vectors have small x components indicating possible cooperative behavior between the group of defects in the region $0.2 \leq x \leq 0.4$, $0.2 \leq y \leq 0.8$ and those in the region $0.6 \leq x \leq 0.8$; $0.2 \leq y \leq 0.8$.

In fig. 7 the average desorption rates $\mathscr{D}$ for the three geometries shown in fig. 6 are plotted. For both the circular and the random defect distributions the average desorption rate decreased relative to the two parallel line-defects. This is evidence of cooperative behavior, which reduces the saturation effect and yields a more efficient trap of material. The fact that the random distribution in this case behaved in the same way as the circular defect structure is probably due to the relatively high density of defects in the region $0.2 \leq x,\ y \leq 0.8$.

5. Conclusions and comments

In this paper we have proposed a numerical algorithm based on the boundary element technique for solving the linear diffusion–desorption equations with generally non-linear reactions occurring on arbitrarily shaped defect structures. The decoupling of linear and non-linear effects in the boundary integral formulation enables defect structures to be incorporated by merely overlaying the effects of the defect structures without deforming the mesh required to evolve the linear part of the solution. This feature together with the use of constant time-steps allows the influence coefficients to be calculated a priori and stored for the evolution process. This saves on transcendental manipulations that would otherwise have to be performed at each step of the evolution process. An explicit scheme is proposed to evolve the non-linear localized effects. The scheme circumvents the need to solve systems of non-linear equations at each time-step. The convergence properties of these schemes have been investigated [13] for one-dimensional models of the two-dimensional surfaces considered in this paper.

If larger problems requiring many more mesh points were to be considered, then more efficient techniques would have to be developed to perform the convolution sums that result from discretizing (3.1). There are two possible techniques that could be employed: (1) The rapid spatial decay of the Green's function (3.2) could be exploited by lumping neighboring cells into regions that are used to propagate effects to remote parts of the mesh. (2) The fast Fourier transform algorithm (FFT) could be exploited to perform the convolution sums [17] by multiplying in frequency space and inverse-transforming the result. These economization schemes could then be used to evolve the linear part of the solution, while the non-linear effect of defect structures can be incorporated by exploiting the overlay feature of the boundary element technique proposed here.

The BE algorithm described was applied to investigate the competitive/cooperative effects that result from changes in defect geometry. In this study the work of the current authors [14] on competitive/cooperative phenomena of reactive trapping defects on one-dimensional surfaces has been extended to two-dimensional surfaces. The competitive/cooperative phenomena were shown to persist on two-dimensional surfaces, while a number of additional interesting effects particular to two-dimensional situations were observed. Reduced competitiveness was observed in the case of random perturbations to a line defect structure. This effect, which was opposite to the trend for more regularly shaped defect structures, emphasizes the richer family of defect structures that can exist in two dimensions compared with the one-dimensional defect structures considered previously. Another particularly interesting phenomenon was the relative competitive effect that was seen to occur in the case of V-shaped defect structures. This phenomenon could be explained by

applying the results of the one-dimensional theory in which a maximum competitiveness was observed for non-zero values of defect spacing. This maximum causes a redistribution of material along the length of the V-shaped defects in a way that reflects the relative competitiveness of the defects on opposite sides of the defect structure.

The BE algorithm is thus shown to be a useful algorithm for modelling the effect of defect structures on active surfaces. In addition, a variety of interesting competitive/cooperative phenomena have been observed for active surfaces exhibiting defect structures.

Acknowledgements

The authors acknowledge support for this research from the Office of Naval Research and the Air Force Office of Scientific Research. The first author also gratefully acknowledges the support of the CSIR of South Africa and the Fulbright Foundation.

Appendix A

A.1. Cell influence coefficients

Assuming piecewise constant representation of the solution in the cells $\mathscr{S}_{mn} = \{(x, y): 2(m-1)a \le x \le 2ma;\ 2(n-1)b \le y \le 2nb\}$, the expression for the influence coefficients (for the cell S_{00}) defined by

$$\overset{\square}{G}{}^{00}_{ij}(x, y, t) = \delta_{ij}\int_{-a}^{a}\int_{-b}^{b} \frac{\exp\left\{-\left[(x-\xi)^2 + (y-\eta)^2\right]/4D_i t - \Omega_i t\right\}}{4D_i \pi t} \mathrm{d}\xi\, \mathrm{d}\eta, \tag{A.1}$$

can be used to generate all the inter-cell influence coefficients by a simple translation of coordinates. The analytic expression for the influence coefficients in (A.1) is

$$\overset{\square}{G}{}^{00}_{ij}(x, y, t) = \frac{\delta_{ij}}{4} e^{-\Omega_i t}\left[\operatorname{erf}\left(\frac{x+a}{2\sqrt{D_i t}}\right) - \operatorname{erf}\left(\frac{x-a}{2\sqrt{D_i t}}\right)\right]\left[\operatorname{erf}\left(\frac{y+a}{2\sqrt{D_i t}}\right) - \operatorname{erf}\left(\frac{y-a}{2\sqrt{D_i t}}\right)\right], \tag{A.2}$$

where

$$\operatorname{erf}(x) = \frac{2}{\sqrt{\pi}} \int_x^\infty e^{-s^2}\, ds$$

and

$$\delta_{ij} = \begin{cases} 1, & i = j, \\ 0, & i \neq j. \end{cases}$$

A.2. Boundary element influence coefficients

We assume a piecewise constant representation of the solution and its normal derivative along boundary line elements and defect line segments. The influence coefficients to determine the effect of the normal derivative $\partial u/\partial n$ in (3.1), which has a constant value along the line segment $-a \leq x \leq a$, $y = 0$ at a point (x, y), is given by the following integral:

$$\bar{G}_{ij}(x, y, t) = \delta_{ij} \int_0^t \int_{-a}^a \frac{\exp\left\{-\left[(x-\xi)^2 + y^2\right]/4D_i(t-\tau) - \Omega_i(t-\tau)\right\}}{4\pi D_i(t-\tau)} d\xi\, d\tau. \quad \text{(A.3)}$$

Here the outward normal is in the direction $(n_1, n_2) = (0, -1)$. The influence coefficients defined in (A.3) are also used to determine the effect of the reaction defined by $R_i(u)$ in (3.1) along the line segment $-a \leq x \leq a$, $y = 0$ on a remote point (x, y). The calculation of influences due to arbitrarily oriented line segments is determined by a rotation of coordinates.

The influence coefficients to determine the effect of the solution u in (3.1) along the line segment $-a \leq x \leq a$ at a point (x, y) is given by the following integral:

$$\bar{F}_{ij}(x, y, t) = -\frac{y\delta_{ij}}{8\pi D_i^2} \int_0^t \int_{-a}^a \frac{\exp\left\{-\left[(x-\xi)^2 + y^2\right]/4D_i(t-\tau) - \Omega_i(t-\tau)\right\}}{(t-\tau)^2} d\xi\, d\tau. \quad \text{(A.4)}$$

Here it is assumed that the normal used to calculate the derivative of the Green's function is in the direction $(n_1, n_2) = (0, -1)$. The calculation of influences due to arbitrarily oriented line segments can be determined by a rotation of coordinates.

Owing to the singular nature of the integrands in (A.3) and (A.4), special care has to be taken when evaluating these integrals for $-a \leq x \leq a$ and $y = 0$. These influence coefficients we shall refer to as self-effects. Evaluating

the spatial integral in (A.3) the self-effects $\bar{G}_{ij}(x, 0, t)$ can be expressed in the following form suitable for numerical approximation:

$$\bar{G}_{ij}(x, 0, t)$$

$$= \frac{\delta_{ij}}{2(\pi D_i \Omega_i)^{1/2}} \int_0^{(\Omega t)^{1/2}} e^{-\tau^2} \left\{ \operatorname{erf}\left[\frac{x+a}{2\tau} \left(\frac{\Omega_i}{D_i} \right)^{1/2} \right] - \operatorname{erf}\left[\frac{x-a}{2\tau} \left(\frac{\Omega_i}{D_i} \right)^{1/2} \right] \right\} d\tau,$$

$$\Omega \neq 0, \tag{A.5a}$$

$$\bar{G}_{ij}(x, 0, t) = \frac{\delta_{ij}}{2(\pi D_i)^{1/2}} \int_0^{t^{1/2}} \operatorname{erf}\left(\frac{x+a}{2 D_i^{1/2} \tau} \right) - \operatorname{erf}\left(\frac{x-a}{2 D_i^{1/2} \tau} \right) d\tau,$$

$$\Omega = 0. \tag{A.5b}$$

We use a limiting technique to evaluate the self-effects $\bar{F}_{ij}(x, 0, t)$. Firstly, the time integral in (A.4) is split into two integrals by considering the intervals $[0, t-\delta]$ and $[t-\delta, t]$ where $\delta \ll t$. The first of these integrals can be shown to vanish as $y \to 0$. The remaining integral can be shown to have the following limiting form:

$$\bar{F}_{ij}(x, \epsilon, t) \overset{\epsilon \to 0}{\sim} \begin{cases} 0, & |x| \geq a, \\ -\dfrac{\operatorname{sign}(\epsilon)\delta_{ij}}{2D_i}, & |x| < a. \end{cases} \tag{A.6}$$

This is essentially the limiting procedure used to obtain the value of $\gamma(x) = \frac{1}{2}$ in (3.1) for $x \in \Gamma$ when Γ is smooth.

The evaluation of $\bar{G}_{ij}$ and $\bar{F}_{ij}$ for points away from the line elements can be evaluated numerically since the integrands in (A.3) and (A.4) are not singular in this case.

References

[1] J.A. Serri, J.C. Tully and M.J. Cardillo, J. Chem. Phys. 79 (1985) 1530.
[2] A.P. Peirce and H. Rabitz, paper in preparation.
[3] D.L. Freeman and J.C. Doll, J. Chem. Phys. 78 (1983) 6002; 79 (1983) 2343.
[4] R.I. Cukier, J. Chem. Phys. 79 (1983) 2430.
[5] E.K. Bimpong-Bota, p. Ortoleva and J. Ross, J. Chem. Phys. 60 (1974) 3124.
[6] E.K. Bimpong-Bota, A. Nitzan, P. Ortoleva and J. Ross, J. Chem. Phys. 66 (1977) 3650.
[7] F.F. Grinstein, H. Rabitz and A. Askar, J. Chem. Phys. 82 (1985) 3430.
[8] D. Lee, A. Askar and H. Rabitz, to be published.
[9] A.P. Peirce and H. Rabitz, Surface Sci. 202 (1988) 1.
[10] P.K. Banerjee and R. Butterfield, Boundary Element Methods in Engineering Science (McGraw-Hill, London, 1981).
[11] C.A. Brebbia and S. Walker, Boundary Element Techniques in Engineering (Newnes–Butterworth, London, 1980).

[12] H.L.G. Pina and J.L.M. Fernandes, Applications in Transient Heat Conduction, in: Vol. 1 of Topics in Boundary Element Research, Ed. C.A. Bebbia (Springer, Berlin, 1984).
[13] A.P. Peirce, A. Askar and H. Rabitz, Surface Sci., to be published.
[14] A.P. Peirce and H. Rabitz, Phys. Rev. B, in press.
[15] W.E. Williams, Partial Differential Equations (Oxford University Press, New York, 1980).
[16] F. John, Partial Differential Equations, 4th ed. (Springer, New York, 1985).
[17] W. Press, B.P. Flannery, S.A. Teukolsky and W.T. Veterling, Numerical Recipes (Cambridge University Press, Cambridge, 1986).